Int J Thermophys (2012) 33:2230–2236
DOI 10.1007/s10765-012-1312-z

Modeling of Thermal-Wave Fields in Radially Inhomogeneous Spherical Solids Using the Green Function Method

Jie Zhang · Guangxi Xie · Chinhua Wang · Andreas Mandelis

Received: 13 February 2012 / Accepted: 20 September 2012 / Published online: 4 October 2012

Abstract A theoretical model for evaluating solid multilayered spherical solids heated by a frequency-modulated light beam using the Green function method is presented. The specific thermal-wave Green function corresponding to the composite structure has been derived. The characteristics of the thermal-wave field with respect to the thermophysical, geometrical, and measurement parameters are presented. Unlike the quadrupole method, the Green function method is capable of evaluating thermal-wave fields at any point of multilayered structures with arbitrary intensity distributions of the incident laser beams. This study establishes applications of thermal-wave fields in both cylindrical and spherical samples using the Green function method and is of importance in characterizing radially inhomogeneous spherical solids.

Keywords Curvilinear surface · Green function method · Multilayered spherical solid · Thermal-wave field

J. Zhang · G. Xie · C. Wang (✉)
Key Lab of Modern Optical Technologies of Jiangsu Province,
Institute of Modern Optical Technologies, Soochow University,
Suzhou, 215006 Jiangsu, People's Republic of China
e-mail: chinhua.wang@suda.edu.cn

G. Xie
Department of Physics, Jiangnan University, Wuxi, 214122 Jiangsu,
People's Republic of China

A. Mandelis
Center for Advanced Diffusion-Wave Technologies (CADIFT), Department of Mechanical and Industrial Engineering, University of Toronto, Toronto, ON M5S 3G8, Canada

1 Introduction

Since their emergence in the 1970s, photothermal techniques have become very powerful tools for the thermophysical characterization and nondestructive evaluation (NDE) of a wide variety of materials [1–5] because of their nondestructive and highly sensitive nature. For decades, research in photothermal techniques has been restricted to samples with flat surfaces. Specifically, with the increasing applications of photothermal radiometry (PTR) to the characterization of materials with curved surfaces, studies on nonflat (e.g., cylindrical or spherical) solids [6–13] have been reported in recent years. In this study, we present a generalized theoretical model of a multilayered spherical structure using the Green function method. An analytical expression for the thermal-wave field in such a multilayered spherical solid is given, and the characteristics of the thermal-wave field with respect to the thermophysical, geometrical, and measurable parameters of the spherical solid are discussed.

2 Theory

The thermal-wave field of a multilayered spherical solid sample with an outer radius $r_N = b$ and inner radii $r_{N-1}, r_{N-2}, \ldots, r_1$, $(b = r_N > r_{N-1} > r_{N-2} > \cdots > r_1 = a)$ can be derived by means of the Green function method. The geometry and coordinates of the boundary-value problem are shown in Fig. 1. The thermal conductivity and thermal diffusivity of regions 1, 2,…,N are denoted by (k_1, α_1), (k_2, α_2),..., and (k_N, α_N), respectively. The harmonic thermal-wave equation for the material under investigation in region N can be written as

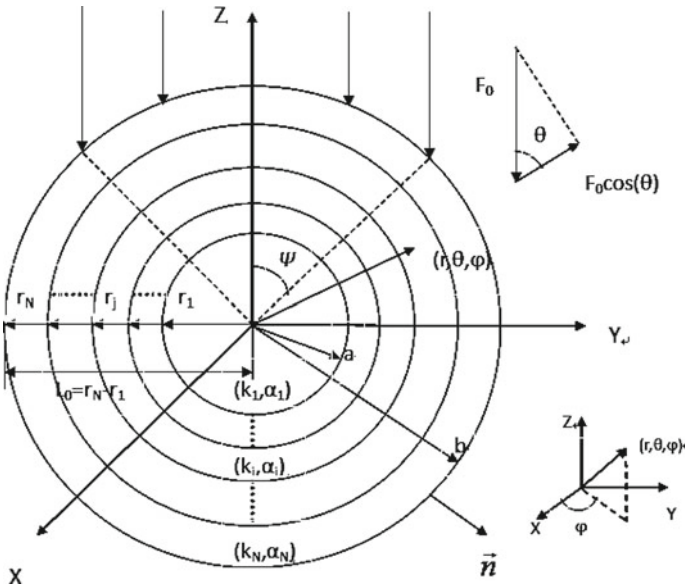

Fig. 1 Geometry and coordinates of a multilayered spherical sample

$$\nabla^2 T(\vec{r},\omega) - \sigma_N^2(\omega) T(\vec{r},\omega) = -\frac{1}{k_N} Q(\vec{r},\omega) \tag{1}$$

where $\sigma_N(\omega) = (\mathrm{i}\omega/\alpha_N)^{1/2} = (1+\mathrm{i})\sqrt{\omega/2\alpha_N}$ is the complex thermal wavenumber, ω is the angular modulation frequency of the laser beam, and $Q(\vec{r},\omega)$ is the volume thermal source at coordinates $\vec{r} = (r,\theta,\varphi)$ inside the material. Based on the Green function method, and considering no volume source ($Q(\vec{r},\omega) \equiv 0$) and no incident flux at the inner surface $r = r_{N-1}$ ($F_{N-1}(\vec{r}_0^{\,s},\omega) = 0$), the general solution for Eq. 1 can be expressed as [14]

$$T(\vec{r},\omega) = \frac{\alpha_N}{k_N} \oint_{S_N} F_N(\vec{r}_0^{\,s},\omega) G^{(N)}(\vec{r}|\vec{r}_0^{\,s},\omega) \mathrm{d}S_0 \tag{2}$$

where $\mathrm{d}S_0$ is the surface element and $\vec{r}_0^{\,s}$ stands for a surface tracing coordinate. The homogeneous boundary conditions for the appropriate Green function and inhomogeneous boundary conditions for the temperature field, respectively, can be written as

$$k_N \vec{n} \cdot \nabla G^{(N)}(\vec{r}\,|\vec{r}_0,\omega)\,\big|_{r=r_{N-1}} = h_{N-1} G^{(N)}(\vec{r}\,|\vec{r}_0,\omega)\,\big|_{r=r_{N-1}} \tag{3a}$$

$$k_N \vec{n} \cdot \nabla G^{(N)}(\vec{r}\,|\vec{r}_0,\omega)\,|_{r=b} = 0 \tag{3b}$$

$$-k_N \vec{n} \cdot \nabla T(\vec{r}\,|\vec{r}_0,\omega)\,\big|_{r=r_{N-1}} = F_{N-1}(\vec{r}_0,\omega) - h_{N-1} T(\vec{r}\,|\vec{r}_0,\omega)\,\big|_{r=r_{N-1}} \tag{4a}$$

$$-k_N \vec{n} \cdot \nabla T(\vec{r}\,|\vec{r}_0,\omega)\,|_{r=b} = F_N(\vec{r}\,|\vec{r}_0,\omega)\,|_{r=b} \tag{4b}$$

where h_{N-1} ($\mathrm{W}\cdot\mathrm{m}^{-2}\cdot\mathrm{K}^{-1}$) is the heat transfer coefficient at the inner surface S_{N-1}, and F_{N-1} and F_N are the heat fluxes ($\mathrm{W}\cdot\mathrm{m}^{-2}$) imposed on the inner and outer surfaces, respectively. After some algebraic calculations, the appropriate Green function to be used in Eq. 2 can be derived and written in the form,

$$G^{(N)}(\vec{r}|\vec{r}_0;\omega) = \frac{\sigma_N}{4\pi\alpha_N} \sum_{l=0}^{\infty} \frac{N_l(\theta) N_l(\theta_0)}{[Y_l(r_N) - X_l(r_{N-1})]} \times \begin{cases} [n_l(\kappa_N r_0) - Y_l(r_N) j_l(\kappa_N r_0)]\,[n_l(\kappa_N r) - X_l(r_{N-1}) j_l(\kappa_N r)], \\ (r_{N-1} \le r \le r_0) \\ [n_l(\kappa_N r_0) - X_l(r_N - 1) j_l(\kappa_N r_0)]\,[n_l(\kappa_N r) - Y_l(r_N) j(\kappa_N r)], \\ (r_0 \le r \le r_N) \end{cases} \tag{5}$$

where

$$X_l(r_{N-1}) \equiv \frac{[n_l'(\kappa_N r_{N-1}) - m_{N-1} n_l(\kappa_N r_{N-1})]}{[j_l'(\kappa_N r_{N-1}) - m_{N-1} j_l(\kappa_N r_{N-1})]}, \quad Y_l(r_N) \equiv \frac{n_l'(\kappa_N r_N)}{j_l'(\kappa_N r_N)} \tag{6}$$

$$m_{N-1} = \frac{[j_l'(\kappa_{N-1} r_{N-1}) + n_l'(\kappa_{N-1} r_{N-1}) \gamma_{(N-1)\ldots 321}]}{\beta_{N,(N-1)}[j_l(\kappa_{N-1} r_{N-1}) + n_l(\kappa_{N-1} r_{N-1}) \gamma_{(N-1)\ldots 321}]}, \quad \text{and } \beta_{N,(N-1)} \equiv k_N / k_{N-1} \tag{7}$$

$\kappa_j \equiv \mathrm{i}\sigma_j = -(1-\mathrm{i})\sqrt{\omega/2\alpha_j}, (j = 1, 2, \ldots, N)$ are thermal wavenumbers. $\gamma_{(N-1)\ldots321} \equiv \frac{t_{21}^{(N-1)}}{t_{11}^{(N-1)}}$, $t_{21}^{(N-1)}$, and $t_{11}^{(N-1)}$ are elements of a matrix representing the recursive relation of thermal properties from layer 1 to layer N, which is similar to that in the N-layer cylindrical case [10]. $N_l(\theta) = \sqrt{\frac{2l+1}{2}} P_l(\cos\theta)$, $P_l(\cos\theta)$ is a Legendre polynomial. $j_l(z)$, $j_l'(z)$ and $n_l(z)$, $n_l'(z)$ are spherical Bessel functions of the first- and second-order kind l, of a complex argument and their derivatives, respectively. In our case, the incident flux prescribed at the outer surface can be written as

$$F_N(r_N, \theta, \varphi, \omega) = \begin{cases} \frac{1}{2} F_0 \cos\theta, \ 0 \le \theta \le \psi, \ 0 \le \varphi \le 2\pi \\ 0, \ \psi \le \theta \le \pi, \ 0 \le \varphi \le 2\pi. \end{cases} \tag{8}$$

After the integration of Eq. 2, the final thermal-wave field is

$$\begin{aligned} T(\vec{r}, \omega) = \frac{F_0}{4k_N} \Bigg\{ & \frac{[n_0(\kappa_N r) - X_0(r_{N-1}) j_0(\kappa_N r)]}{j_0'(\kappa_N r_N)[Y_0(r_N) - X_0(r_{N-1})]} \frac{\sin^2\psi}{2} \\ & + \frac{[n_1(\kappa_N r) - X_1(r_{N-1}) j_1(\kappa_N r)]}{j_1'(\kappa_N r_N)[Y_1(r_N) - X_1(r_{N-1})]} \cos\theta \ (1 - \cos^3\psi) \\ & \sum_{l=2}^{\infty} \frac{[n_l(\kappa_N r) - X_l(r_{N-1}) j_l(\kappa_N r)]}{j_l'(\kappa_N r_N)[Y_l(r_N) - X_l(r_{N-1})]} \\ & \frac{(2l+1)\sin\psi}{(l-1)(l+2)} P_l(\cos\theta)[\sin\psi \, P_l(\cos\psi) + \cos\psi \, P_l^1(\cos\psi)] \Bigg\} \end{aligned} \tag{9}$$

where P_l, P_l^m denote Legendre polynomials and associated Legendre polynomials, respectively.

3 Numerical Simulations

In all simulations, the amplitude and phase of the surface thermal-wave field are normalized to the corresponding amplitude and phase of a homogeneous flat surface of the same thermophysical properties with semi-infinite thickness (AISI 1018 steel). The thermophysical parameters of AISI 1018 steel are $k = 51.9 \ \mathrm{W \cdot m^{-1} \cdot K^{-1}}$, $\alpha = 13.57 \times 10^{-6} \ \mathrm{m^2 \cdot s^{-1}}$ [15].

We assume that the radial depth profile of the thermal conductivity of an inhomogeneous sphere varies continuously along the radial direction [16]:

$$k(r) = k_0 \left(\frac{1 + \Delta \mathrm{e}^{-Qr}}{1 + \Delta} \right)^2, \quad \text{with } \Delta = \frac{1 - \sqrt{k'/k_0}}{\sqrt{k'/k_0} - \mathrm{e}^{-QL_0}}, \tag{10}$$

where k_0 and k' represent the thermal conductivity of the outermost layer and innermost layer, respectively, L_0 is the thickness of the inhomogeneous surface layer, and exponent Q represents the thermal gradient. Figure 2a shows the assumed thermal-conductivity profiles of two inhomogeneous spherical solids. Figure 2b1, b2 shows

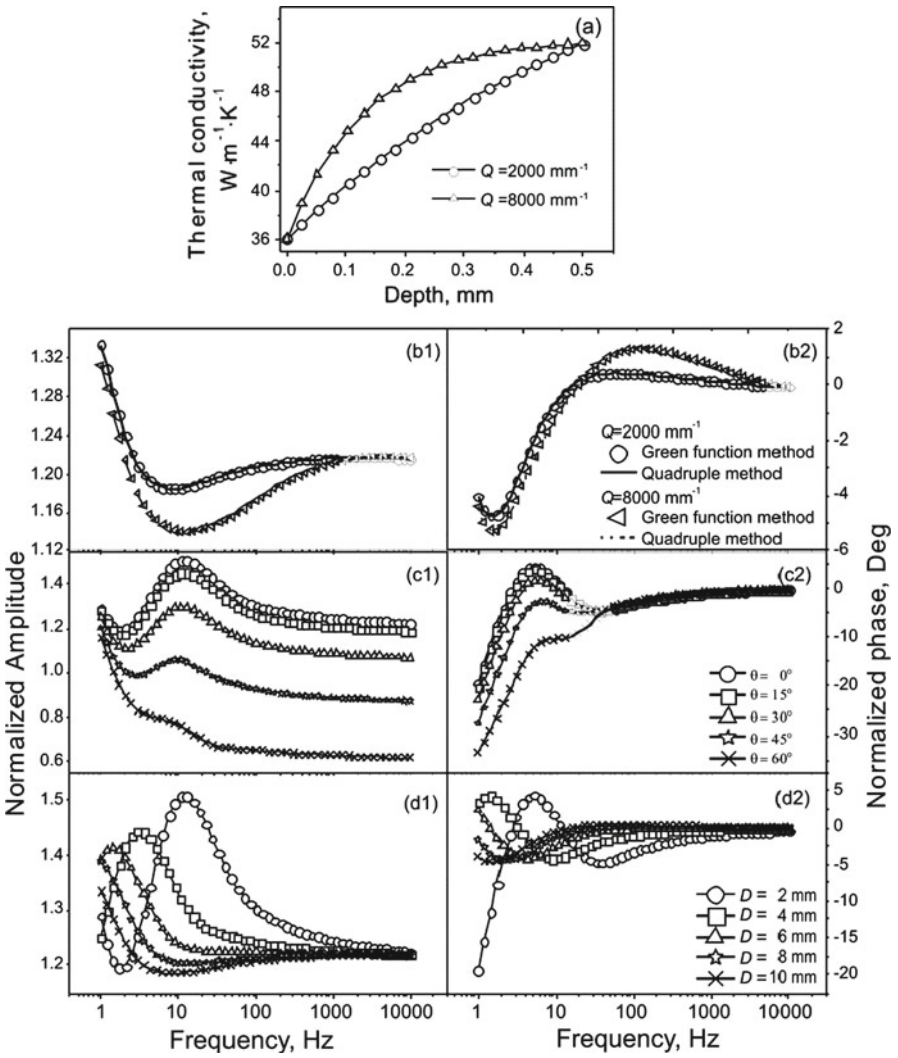

Fig. 2 (a) Assumed thermal-conductivity depth profiles of two inhomogeneous solid spheres with different thermal gradients, Q (mm^{-1}); (b1, b2) thermal-wave responses of two inhomogeneous spheres and comparison with results obtained with the quadrupole method; (c1, c2) normalized amplitude and phase at different azimuthal angles, θ; and (d1, d2) the normalized amplitude and phase of spherical solids with various diameters at $\theta = 0°$

the thermal-wave responses of the two inhomogeneous spheres, diameters = 2 mm with different Q, and the results obtained by the quadrupole method (line) [11] are shown for comparison. Different depth profiles with different Q factors imply different effective thicknesses of the inhomogeneous layer, which result in different peak or valley positions in both amplitude and phase channels. The point where simulated measurements are made is at $\theta = 0°$.

As shown in Eq. 8, the thermal-wave field is also a sensitive function of the geometrical and measurement parameters. Figures 2c1, c2 shows the normalized amplitude and phase of a spherical solid (diameter = 2 mm) at different azimuthal angles θ. Figure 2d1, d2 shows the normalized amplitude and phase of spherical solids with different diameters (D) at $\theta = 0°$. In the simulation, the depth profile of the thermal conductivity in Fig. 2a is used, with $Q = 2000\ \mathrm{mm}^{-1}$. From Fig. 2c1, c2 it is seen that under the same illumination and same geometrical diameter, the thermal-wave field is very sensitive to the measurement angle θ, which suggests that precise alignment is required for quantitative experiments. In Fig. 2d1, d2 it is seen that the thermal-wave signal is more sensitive to frequencies in the middle or low ranges when the diameter of the solid decreases.

4 Conclusions

We have developed a theoretical thermal-wave model that is suitable for characterizing multilayered spherical solids using a laser beam with arbitrary intensity spatial profile. Based on the Green function method, the thermal-wave field from a multilayered spherical solid was obtained. The thermal-wave dependencies on various thermophysical and geometrical parameters were investigated. With the advantages of the Green-function method regarding arbitrariness of the photothermal source spatial profile and its ability to handle both homogeneous and inhomogeneous boundary conditions, this model offers a general analytical tool for characterizing spherical solids with photothermal techniques.

Acknowledgments This study was supported by a grant from the National Natural Science Foundation of China Contract No. 60877063, Scientific Research Foundation for Returned Scholars, Ministry of Education of China, and the project of the Priority Academic Program Development (PAPD) of Jiangsu Higher Education Institutions. The Canada Research Chairs and the Natural Sciences and Engineering Research Council (NSERC) of Canada are gratefully acknowledged for their support through CRC Tier I Awards and Discovery Grants to AM.

References

1. A. Mandelis (ed.), *Non-Destructive Evaluation*, vol. 2 of the series: *Progress in Photothermal and Photoacoustic Science and Technology* (PTR-Prentice Hall, Englewood Cliffs, 1994)
2. H.K. Park, C.P. Grigoropoulos, A.C. Tam, Int. J. Thermophys. **16**, 973 (1995)
3. R. Santos, L.C.M. Miranda, J. Appl. Phys. **52**, 4194 (1981)
4. D.P. Almond, P.M. Patel, *Photothermal Science and Techniques* (Chapman and Hall, London, 1996)
5. L. Fabbri, P. Fenici, Rev. Sci. Instrum. **66**, 3593 (1995)
6. C. Wang, A. Mandelis, Y. Liu, J. Appl. Phys. **96**, 3756 (2004)
7. C. Wang, A. Mandelis, Rev. Sci. Instrum. **78**, 054902 (2007)
8. C. Wang, Y. Liu, A. Mandelis, J. Shen, J. Appl. Phys. **101**, 083503 (2007)
9. G. Xie, Z. Chen, C. Wang, A. Mandelis, Rev. Sci. Instrum. **80**, 034903 (2009)
10. G. Xie, J. Zhang, L. Liu, C. Wang, A. Mandelis, J. Appl. Phys. **109**, 113534 (2011)
11. A. Salazar, F. Garrido, R. Celorrio, J. Appl. Phys. **99**, 066116 (2006)
12. A. Salazar, R. Celorrio, J. Appl. Phys. **100**, 11355 (2006)
13. N. Madariaga, A. Salazar, J. Appl. Phys. **01**, 103534 (2007)
14. A. Mandelis, *Diffusion-Wave Fields: Mathematical Methods and Green Function* (Springer, New York, 2001), pp. 85, 90, 200

15. R. Steiner, Properties of Selection: Iron, Steel of High Performance Alloys, in *Metals Handbook*, vol. 1, 10th edn. (ASM International, Materials Park, Ohio, 1990), p. 196
16. A. Mandelis, F. Funak, M. Munidasa, J. Appl. Phys. **80**, 5570 (1996)